Letter

A-Source Impedance Network

Yam P. Siwakoti, *Member, IEEE*, Frede Blaabjerg, *Fellow, IEEE*, Veda Prakash Galigekere, *Member, IEEE*, Agasthya Ayachit, and Marian K. Kazimierczuk, *Fellow, IEEE*

***Abstract*—A novel A-source impedance network is proposed in this letter. The A-source impedance network uses an autotransformer for realizing converters for any application that demand a very high dc voltage gain. The network utilizes a minimal turns ratio compared to other magnetically coupled impedance source networks to attain a high voltage gain. In addition, the proposed converter draws a continuous current from the source, and hence it is suitable for many types of renewable energy sources. The derived network expressions and theoretical analysis are finally validated experimentally with an example single-switch 400-W dc–dc converter. For the closed-loop control design and stability assessment, a small signal model and its analysis of the proposed network are also presented in brief.**

***Index Terms*—ac–ac power conversion, ac–dc power conversion, dc–dc power conversion, dc–ac power conversion, magnetically coupled impedance source (MCIS) network, Y-source network, Z-source network.**

I. Introduction

VARIOUS impedance source network topologies have been reported in the literature to improve the performance of power converters, especially where it requires a high voltage boost in a single-stage power conversion [1]. The Z-source network being the first in the series with quasi-Z-source network and several other networks with multiple active and passive elements. These include a network with switched-inductor or switched-capacitor, cascaded with diode and/or capacitor assisted, and coupled magnetics [1]–[3]. Compared to the former two techniques, the coupled magnetics reduce the number of components, while improving the boost capability and power density of the converter. This means that higher modulation index and voltage gain can be achieved simultaneously for dc–ac systems, which lowers the dc-link voltage required to produce a high gain, and hence lower the stresses experienced by the switches. Some popular two winding magnetically coupled impedance source (MCIS) networks includes the Γ-Z-source [4], flipped-Γ-Z-source [2], T-source [5], trans-Z-source [6], TZ-source [7], LCCT-Z-source/quasi-LCCT-Z-source [8], and LCCAt [9]. Recently, a three-winding network called the Y-source network [10] and quasi Y-Source network have also been introduced. Each of these networks has its own characteristic features, which are helpful depending on the application under consideration.

In this paper, a two-winding MCIS network is proposed to reduce the number of turns required to achieve a higher output voltage without compromising the performance and component count. Compared to two-winding or three-winding MCIS networks aforementioned, the proposed network uses an autotransformer principle and considerably reduces the turns ratio. Therefore, its power density can be improved and the cost of the system can be reduced. The circuit topology, its principle of operation with mathematical derivation, and its small-signal model are documented in Section II. Its realization as a single-switch dc–dc converter is then discussed in Section III with some simulation and experimental results. Conclusions and verification of the anticipated results are provided in Section IV.

Manuscript received April 26, 2016; revised May 23, 2016; accepted June 08, 2016. Date of publication June 10, 2016; date of current version July 08, 2016.

Y. P. Siwakoti and F. Blaabjerg are with the Department of Energy Technology, Aalborg University, Pontoppidanstræde 101, 9220, Aalborg Denmark (e-mail: yas@et.aau.dk; fbl@et.aau.dk).

V. P. Galigekere is with the Electrical Power Management Systems, Lear Corporation, Southfield, MI 4033 USA (e-mail: galigekere.2@wright.edu).

A. Ayachit is with the Department of Electrical Engineering, Wright State University, Dayton, OH 45435 USA (e-mail: ayachit.2@wright.edu).

M. K. Kazimierczuk is with the Department of Electrical Engineering, Wright State University, Dayton, OH 45435 USA (e-mail: marian.kazimierczuk@wright.edu).

Color versions of one or more of the figures in this paper are available online at http://ieeexplore.ieee.org.

Digital Object Identifier 10.1109/TPEL.2016.2579659

II. Proposed Topology and Principle of Operation

A. Circuit Description

Fig. 1(a) shows the circuit of the A-Source impedance network. It consists of an inductor L, two capacitors C_1 and C_2, an autotransformer with N_1, L_1 and N_2, L_2 being the primary and the secondary turns and the inductances, respectively, a controlled switch SW and diode D_1. The maximum output voltage of the A-Source network is represented by V_{om}. Depending on the requirement, an inverter or a filter network can be incorporated at the nodes depicting V_{om} to obtain either a dc–ac inverter or a dc–dc converter. In principle, the A-Source network can be utilized for dc–ac, dc–dc, ac–dc, or ac–ac energy conversion.

The active switch SW, typically a MOSFET, is switched at a switching frequency of $f_s = \frac{1}{T_s}$, where T_s is the switching time period. The duty cycle of the switch SW is $D_{st} = \frac{t_{on}}{T_s}$. The duty cycle recreates the shoot-through state of the A-Source inverter similar to the shoot-through state in [1].

The aforesaid network and its winding are based on the principle of an autotransformer. Fig. 2 shows the basic difference between normal wound coupled inductor, which is used in other conventional impedance source networks and autotransformer type wound coupled inductor. Using the principle of an autotransformer, the coupled inductor shown in Fig. 2(b) can achieve higher voltage gain ($\mathrm{V_2/V_1 = N = n + 1}$) as compared to normal coupled inductor ($V_2/V_1 = n$) shown in Fig. 2(a). Such a simple modification in the winding design and its arrangement with switching devices can help the network to achieve a unique and unmatched voltage gain capability. However, the coupling

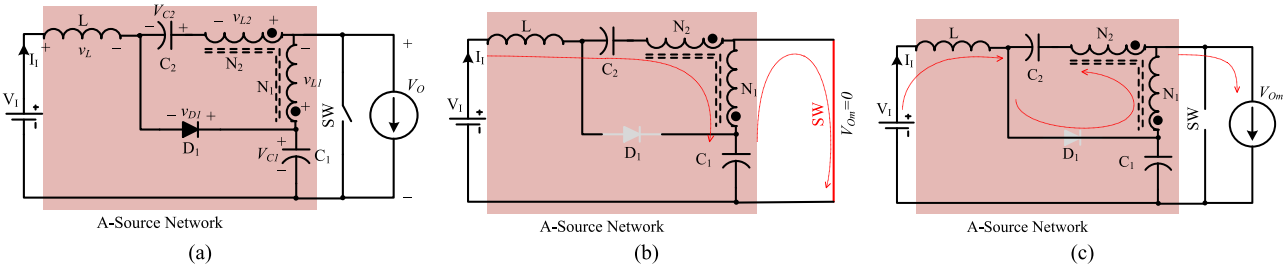

Fig. 1. Illustration of (a) A-source impedance network and its equivalent circuits during, (b) shoot-through, and (c) non-shoot-through states.

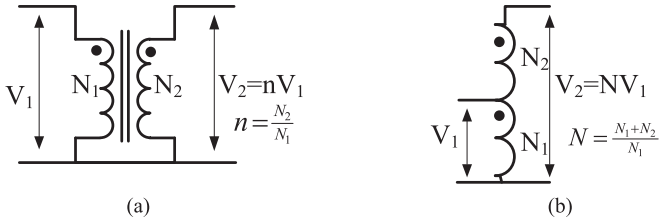

Fig. 2. (a) Schematic illustrating the autotransformer type coupled inductor and a normal coupled inductor.

of the windings must be tight to ensure very small leakage inductances at its winding terminals. This can be done by following the winding style used in [2] and [10].

B. Shoot-Through State

The equivalent circuit of the A-Source network during the shoot-through state is shown in Fig. 1(b). During the shoot-through state the switch SW is ON and the diode D_1 is OFF. By applying KVL to Fig. 1(b), we get

$$V_I - v_L + V_{C2} + \frac{N_2}{N_1} v_{L1} + v_{L1} - V_{C1} = 0 \tag{1}$$

and

$$v_{L1} = V_{C1}. \tag{2}$$

By rearranging (1), we obtain

$$v_L = V_I + V_{C2} + v_{L1}\left(\frac{N_2}{N_1} + 1\right) - V_{C1}. \tag{3}$$

From (2) and (3), the voltage across the inductor L during the shoot-through state is

$$v_L = V_I + V_{C2} + \frac{N_2}{N_1} V_{C1}. \tag{4}$$

C. Non-Shoot-Through State

The equivalent circuit of the A-Source network during the nonshoot through state is shown in Fig. 1(c). In this state, the switch SW is OFF and the diode D_1 is forward biased. The state equations are

$$v_L = V_I - V_{C1} \tag{5}$$

and

$$V_{C2} + \frac{N_2}{N_1} v_{L1} + v_{L1} = 0 \tag{6}$$

to give

$$v_{L1} = -\frac{V_{C2}}{\frac{N_2}{N_1} + 1}. \tag{7}$$

Applying the volt-second balance principle to the inductor L_1, we have

$$\int_0^{D_{st}T_s} v_{L1} dt + \int_{D_{st}T_s}^{T_s} v_{L1} dt = 0. \tag{8}$$

Substituting (2) and (7) into (8) results in

$$V_{c1} D_{st} - \frac{V_{C2}}{\left(1 + \frac{N_2}{N_1}\right)} (1 - D_{st}) = 0 \tag{9}$$

yielding

$$\frac{V_{C1}}{V_{C2}} = \frac{1 - D_{st}}{\left(1 + \frac{N_2}{N_1}\right) D_{st}} \tag{10}$$

where D_{st} represents the shoot-through duty cycle of the switch. Applying the volt-second balance principle to the inductor L leads to

$$\int_0^{D_{st}T_s} v_L dt + \int_{D_{st}T_s}^{T_s} v_L dt = 0. \tag{11}$$

Substituting (3) and (5) into (11) gives

$$\left(V_I + V_{C2} + \frac{N_2}{N_1} V_{C1}\right) D_{st} + (V_I - V_{C1})(1 - D_{st}) = 0 \tag{12}$$

or equivalently

$$V_I + \left[\left(\frac{N_2}{N_1} + 1\right) D_{st} - 1\right] V_{C1} + D_{st} V_{C2} = 0. \tag{13}$$

Solving (10) and (13), the voltage across the capacitors C_1 and C_2 can be found as

$$V_{C1} = \frac{1 - D_{st}}{1 - \left(2 + \frac{N_2}{N_1}\right) D_{st}} V_I = \frac{1 - D_{st}}{1 - (1 + N) D_{st}} V_I \tag{14}$$

$$V_{C2} = \frac{\left(\frac{N_2}{N_1} + 1\right) D_{st}}{1 - \left(2 + \frac{N_2}{N_1}\right) D_{st}} V_I = \frac{N D_{st}}{1 - (1 + N) D_{st}} V_I \tag{15}$$

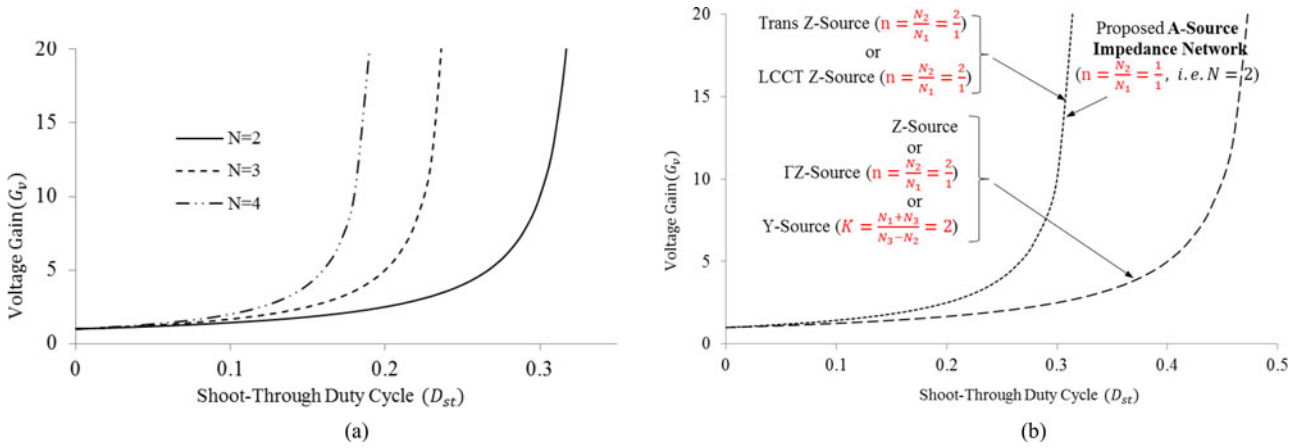

Fig. 3. (a) Theoretical voltage gain G_v of the A-source impedance network as a function of duty cycle D_{st} at selected values of turns ratio $N = \frac{N_1+N_2}{N_1}$ and (b) voltage gain comparison of the proposed A-source impedance network with various conventional impedance source networks.

TABLE I
COMPARISON OF THE PROPOSED A-SOURCE NETWORK WITH SOME CONTINUOUS INPUT CURRENT TYPE TWO WINDINGS MCIS NETWORKS

Topologies	$G_v = V_{om}/V_I$	$0 < D_{st} < D_{\mathrm{stmax}}$	No. of Components			
			L	C	Coupled Inductor	Diode
Quasi-Γ-Z-source [2]	$\left(1 - \frac{N_2}{N_2 - N_3} D_{st}\right)^{-1}$	$0 \le D_{st} < \frac{N_2 - N_3}{N_2}$	1	2	1	1
Quasi-T-source or quasi-Trans-Z-source [2]	$\left(1 - \frac{N_1}{N_3} D_{st}\right)^{-1}$	$0 \le D_{st} < \frac{N_3}{N_1}$	1	2	1	1
Quasi LCCT-Z-source [2]	$\left[1 - \left(1 + \frac{N_1}{N_2}\right) D_{st}\right]^{-1}$	$0 \le D_{st} < \frac{N_2}{N_1 + N_2}$	1	2	1	1
LCCT [8] / LCCTAt [9]	$\left[1 - \left(1 + \frac{N_1}{N_2}\right) D_{st}\right]^{-1}$	$0 \le D_{st} < \frac{N_2}{N_1 + N_2}$	1	2	1	1
Proposed A-Source Network	$\left[1 - \left(2 + \frac{N_2}{N_1}\right) D_{st}\right]^{-1}$	$0 \le D_{st} < \left[2 + \frac{N_2}{N_1}\right]^{-1}$	1	2	1	1

where $N = \frac{N_1+N_2}{N_1}$ is the autotransformer turns ratio.

D. DC Voltage Transfer Ratio

The maximum output voltage achievable during the non-shoot-through period is calculated as follows. During the non-shoot-through period

$$V_{Om} = V_{C1} - v_{L1}. \tag{16}$$

Hence, the voltage transfer ratio G_v to achieve an output voltage of V_{Om} during the non-shoot-through period is found by solving (7), (10), and (14) in (16) as

$$G_v = \frac{V_{om}}{V_I} = \frac{1}{1 - (1+N) D_{st}}. \tag{17}$$

Moreover, by setting the denominator of (17) to be greater than zero, the range of variation for D_{st} of the A-source network can be determined as

$$0 \le D_{st} < D_{\mathrm{stmax}} = \frac{1}{1+N}. \tag{18}$$

Fig. 3(a) shows the plot of the theoretical voltage gain at different autotransformer turns ratios $N = \frac{N_1+N_2}{N_1}$, where $N > 1$ as a function of the shoot-through duty cycle D_{st}. Note that the voltage gain of the proposed A-source impedance source network is higher than that of conventional impedance source networks as shown in Fig. 3(b). The gain of proposed network with just 1:1 turns ratio is higher than the Z-source, ΓZ-source, and Y-source with higher turns ratio or winding factor (2:1) and similar to Trans-Z-source or LCCT Z-source but with higher turns ratio of 2:1. Hence, the proposed impedance source network reduces the turns ratio and hence the size and weight of coupled magnetics compared to conventional impedance source networks for the same gain. Table I summarizes the number of components required and voltage gain of some of the two-winding MCIS networks.

Similar to all the other pulsewidth modulated converters, the principle of energy conservation is applicable for A-Source impedance based converters as well. As a consequence, assuming 100% efficiency, the input-to-output dc current transfer

TABLE II
VOLTAGE AND CURRENT STRESSES ACROSS THE SWITCH AND DIODES IN A-SOURCE DC–DC CONVERTER

Component	Voltage Stress	Current Stress
Switch SW	$V_{\rm DSM} = V_O$	$I_{\rm DSM} = \dfrac{NV_O}{R_L\left[1-(1+N)D_{st}\right]} + \dfrac{N(V_I+V_{C1})}{2f_sL}$
Diode D_1	$V_{\rm D1M} = NV_O$	$I_{\rm D1M} = \dfrac{I_O}{1+\dfrac{N_1}{N_2}} + \dfrac{V_I+V_{C1}}{2f_sL}$
Diode D_2	$V_{\rm D2M} = V_O$	$I_{\rm D2M} = (N+1)I_O$

TABLE III
VOLTAGE STRESSES ACROSS THE CAPACITORS IN A-SOURCE DC–DC CONVERTER

Component	Notation	Equation
Capacitor C_1	V_{C1}	$\dfrac{1-D_{st}}{1-(1+N)D_{st}}V_I$
Capacitor C_2	V_{C2}	$\dfrac{ND_{st}}{1-(1+N)D_{st}}V_I$
Capacitor C_O	V_{CO}	V_O

characteristic during the non-shoot-through period is

$$G_i = \frac{I_{Om}}{I_I} = \frac{1}{G_v} = 1-(1+N)\,D_{st}. \tag{19}$$

E. Component Stress

Table II summarizes the voltage and current stresses of the switch SW and the diodes D_1, D_2 in the A-Source dc–dc converter. The expressions to determine the voltage and current are also provided. Table III provides the voltage stresses across the capacitors C_1, C_2 in the A-Source network and the filter capacitor C_O. The expressions to determine the voltage stresses of C_1 and C_2 have been derived in (14) and (15), respectively.

F. Control Transfer Function

The equations describing the steady-state behavior have been derived in the previous sections. Small-signal analysis similar to [11], [12] is applied in this section to obtain the variation in v_{c1} due to perturbation in D_{st} in the frequency domain. Fig. 4 shows the small-signal model of the A-source network obtained using circuit averaging technique. The controllable switch, here the MOSFET, is replaced by dependent current sources and the diode is replaced by dependent voltage sources. Detailed description on circuit averaging technique for power converters are discussed in [13]–[17]. The expression for the duty cycle-to-capacitor voltage transfer function T_d derived using the small-signal model shown in Fig. 4 is

$$T_d = \frac{v_{c1}}{d} = \frac{\dfrac{B}{1-A} - \dfrac{P}{Z_L} - \dfrac{P}{Z_O N\,(1-A)} - \dfrac{Z_{C2}}{N^2 Z_L\,(1-A)\,Z_O}}{\dfrac{2Z_{C2}}{N^2 Z_L\,(1-A)\,Z_O} - \dfrac{1}{Z_L} - \dfrac{1}{Z_{C1}\,(1-A)} - \dfrac{1}{Z_O\,(1-A)}} \tag{20}$$

where

$$Z_L = sL, \qquad Z_{C1} = \frac{1}{sC_1}, \qquad Z_{C2} = \frac{1}{sC_2}, \qquad Z_O = R_o + sL_o \tag{21}$$

and the constants in the model are

$$A = \frac{D_{st}N}{D'_{st}}, \quad B = \frac{I_I N}{D'^2_{st}}, \quad P = \frac{NV_I}{\left[1-(1+N)\,D_{st}\right]^2}, \tag{22}$$

where $D'_{st} = 1 - D_{st}$.

III. IMPLEMENTATION AND EXAMPLE DC–DC CONVERTER

A dc–dc converter as shown in Fig. 5(a) is implemented using the A-source impedance network, which includes an additional diode D_2, capacitor C_O, and load resistance R_L. In this circuit, the turn-ON of the switch SW causes the diodes D_1 and D_2 to be reverse biased. Simultaneously, C_1 and C_2 charges the magnetizing inductance of the autotransformer and C_O powers the load. On the other hand, the turn-OFF of the switch SW causes diode D_1 to conduct and the supply voltage V_I to recharge C_1 and C_2. The supply voltage together with the autotransformer supplies energy to recharge C_O as well as power the load, only if the voltage V_O across C_O is lower than V_{Om}, where V_{om} is the maximum value of the output voltage. During this interval, D_2 conducts connecting C_O and the load R_L to the rest of the circuit. The cycle repeats when SW turns ON again. By periodically switching SW, the load voltage V_O across C_O can hence be regulated at V_{Om}, which accordingly to (17), represents a gain.

A scaled-down 400-W prototype was built in the laboratory for verifying the performance of the proposed converter. The layout of the converter is shown in Fig. 5(b), while its parameters are summarized in Table IV. Among the listed parameters, $N = 2$ can be substituted to (18) for computing the shoot-through range as $0 < D_{st} < 1/3$. The chosen D_{st} of 0.25 in Table II is, thus, a valid value, which when used will give rise to a computed gain of 4 according to (17). This gain is higher than the conventional MCIS networks using the same turns ratio and duty cycle. The output voltage of the proposed converter will hence be boosted to $V_{om} = 200$ V at an input voltage $V_I = 50$ V. This computed output voltage is indeed the same as that read from the third simulation/experimental trace shown in Fig. 6(a). The converter is also noted to draw continuous current from the source, as seen from the second trace shown in Fig. 6(a). This is definitely different from the pulsating input current drawn by some of the MCIS networks [2]. Hence, the proposed topology with

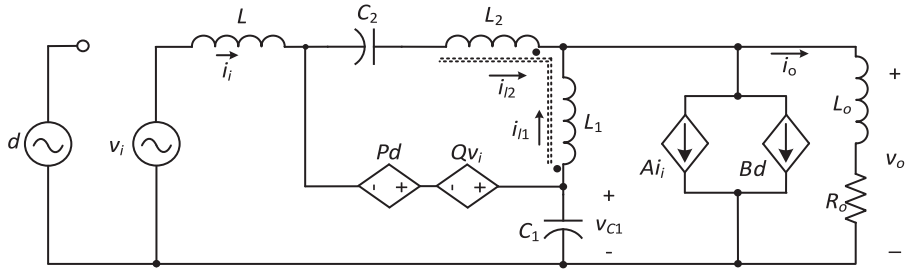

Fig. 4. Small-signal linear model of the A-source impedance network.

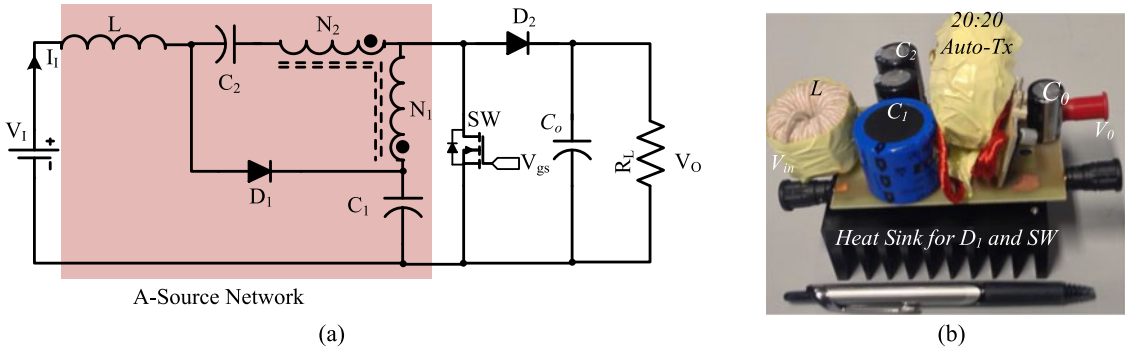

Fig. 5. Implementation of A-source impedance network in a single switch dc–dc converter: (a) schematic circuit and (b) a 400-W prototype.

TABLE IV
TESTED PARAMETERS AND HARDWARE COMPONENTS

Parameter/Description		Value/Part Number
Power rating P_O		400 W
Input voltage V_I		50–150 V
Output voltage V_O		200 V
Capacitor	C_1	100 µF, 400 V, *Kemet*
	C_2	220 µF, 400 V, *Kemet*
	C_O	47 µF, 400 V, *Kemet*
Inductor L		635 µH
Load R_L		200 Ω
Turns ratio $N_2 : N_1$		20:20 = 1:1, *i.e.* $N = 2$
Duty cycle D_{st}		0.1- 0.25
Switching frequency f_s		30 kHz
Switch *SW*		IPW60R041C6
Diode D_1		IDW40G65C5
Diode D_2		STTH16R04C

its continuous input current and high voltage boost is, therefore, more suitable for renewable and distributed power generation. Other simulated and measured amplitudes in Fig. 6(b) have also been noted to be in agreement with theoretical values calculated using expressions derived in Section II, which to a great extent, have verified performances expected from the network.

The efficiency of the dc–dc converter designed with A-source network is shown in Fig. 7(a) over a wide range of input voltages. The shoot-through duty cycle was varied from 0.05 to 0.25 to boost the output voltage at 200 V from wide range of input voltage (50–150 V). The efficiency reduces slightly with increase in shoot-through duty cycle (i.e., with corresponding reduction in input voltage), as it draws a higher current from the source at an elevated boost ratio. Consequently, the associated conduction loss deviates the measured voltage gain from the theoretically expected value at higher voltage gains. For an overview of the converter loss distribution, a thermal image of the experimental prototype operating at 400 W (rated) is also captured in the steady state, as shown in Fig. 7(b). The temperature of the converter stabilizes below 55°C at full load conditions. It should be mentioned here that the 400-W laboratory prototype has been conceived on a proof-of-concept basis. The proposed network is suitable for higher power dc–dc, dc–ac or ac–dc applications using appropriate switching configuration and modulation techniques [2].

Furthermore, the small-signal model and the duty cycle-to-capacitor voltage transfer function discussed in Section II-D were verified by simulations. Fig. 8 shows the theoretically obtained magnitude and phase plots of the duty cycle-to-capacitor voltage transfer function given in (20) and are represented by solid lines. The magnitude plot shows a high gain at dc, $T_d(0) = 64.01$ dB. A low damping yields a high overshoot since the transfer functions in the current form omits parasitic resistances. The phase plot crosses -180^o at approximately 420 Hz. The predicted results were verified by circuit simulations and the results are shown as discrete points in Fig. 8. The discrete points were obtained by perturbing the duty cycle about the operating point in the actual circuit for the specifications given in Table II. A good agreement between the two results can

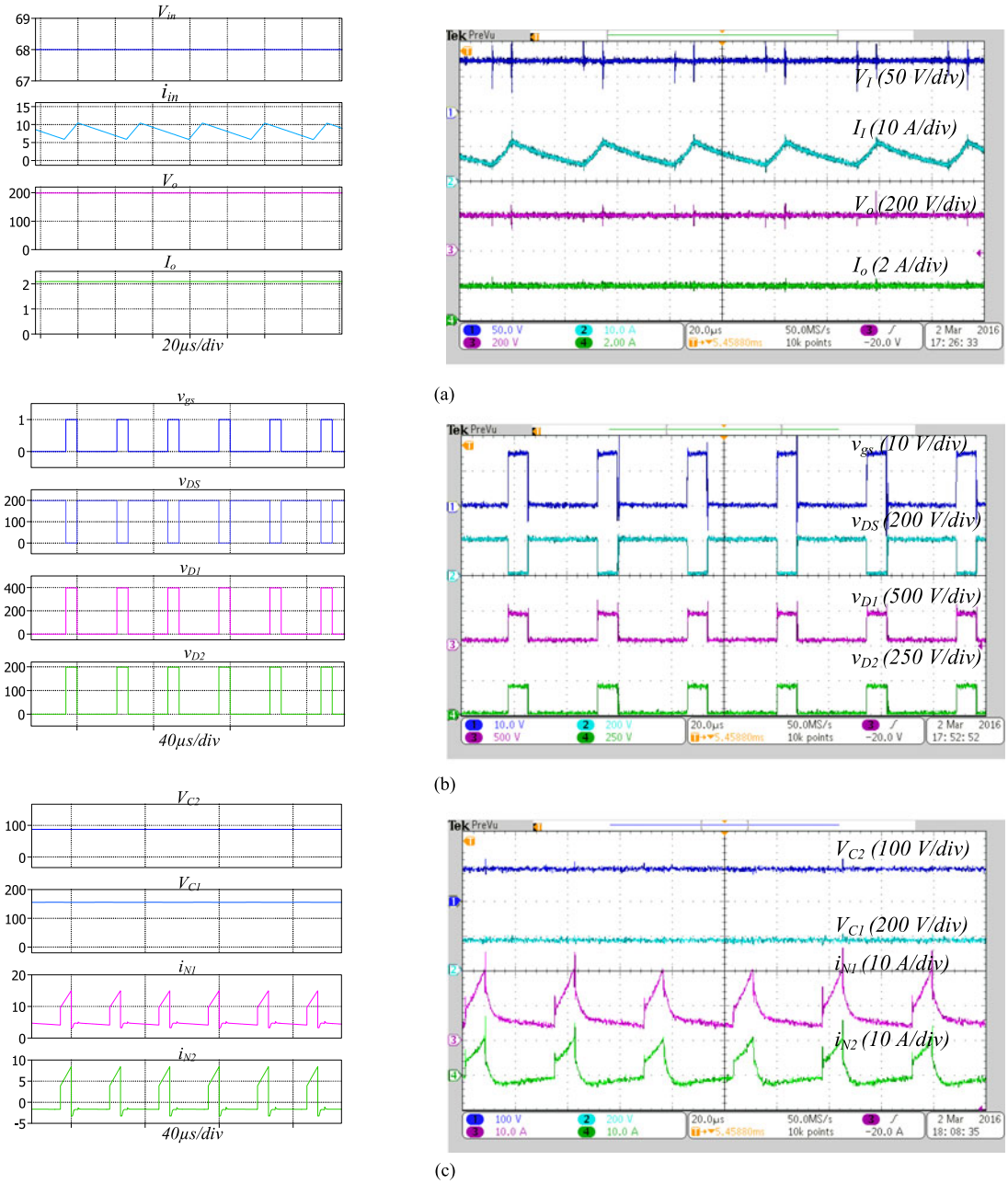

Fig. 6. Simulation (left) and experimental (right) waveforms of the single switch A-source dc–dc converter. (a) Input voltage V_I, input current i_I, output voltage V_O, and output current I_O. (b) Gate-source voltage v_{GS}, drain-source voltage v_{DS}, and voltages across the diodes v_{D1} and v_{D2}. (c) Voltage across the capacitors V_{C1} and V_{C2} and currents through the two windings i_{N1} and i_{N2}.

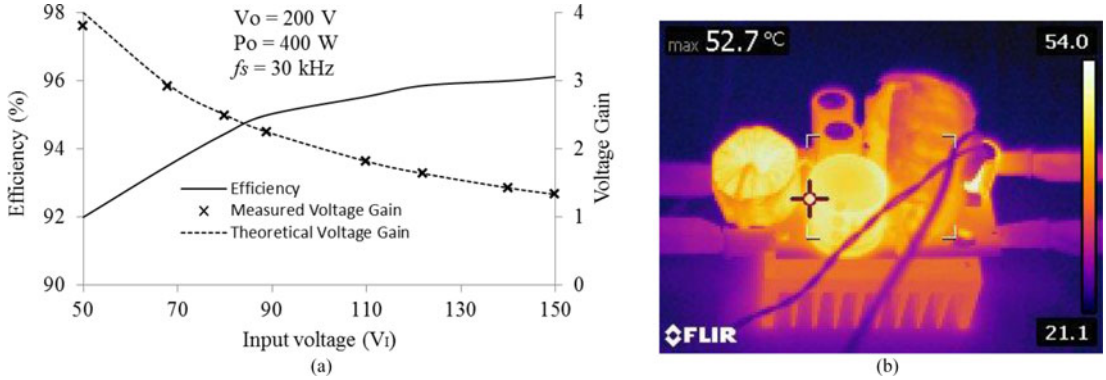

Fig. 7. (a) Measured power conversion efficiency and voltage gain of an example single switch dc–dc converter (shown in Fig. 5) as a function of input voltage (shoot-through duty-cycle) and (b) thermal image showing heat loss and thermal distribution of the converter at a full load conditions.

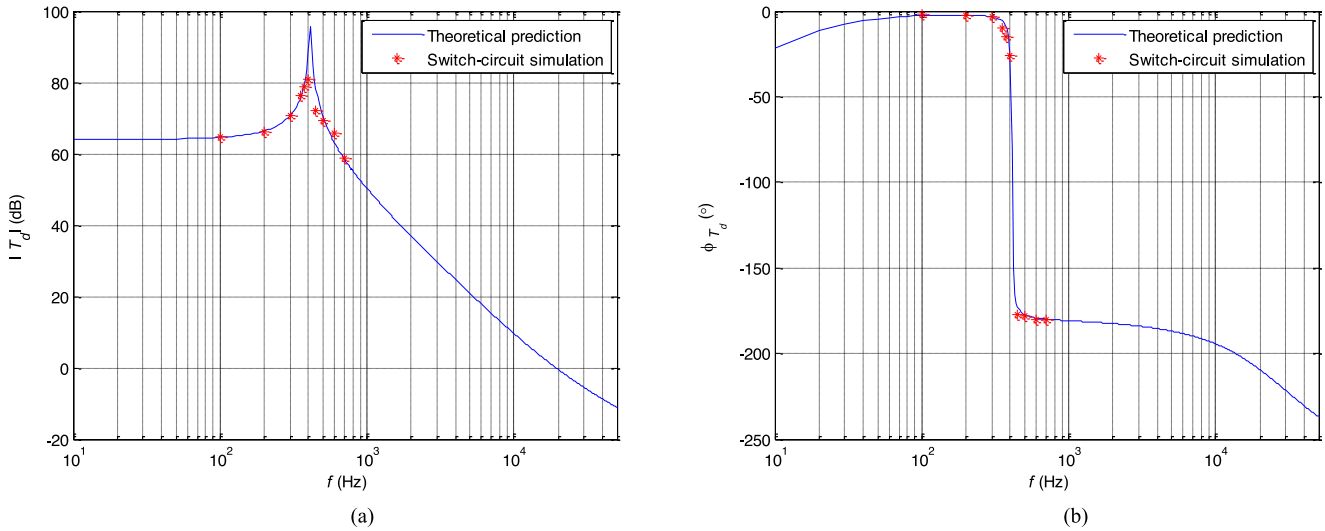

Fig. 8. Comparison of theoretically predicted and simulated Bode plots of the duty cycle-to-capacitor voltage transfer function. (a) Magnitude $|T_d|$. (b) Phase ϕ_{Td}.

be observed confirming the validity of the small-signal analysis. Moreover, the pole-zero plot of the control transfer function showed the presence of a right-half plane zero, a unique characteristic of non-minimum phase systems as also experienced by other impedance source networks and boost dc–dc converter [10], [11]. Single-lead or double-lead integral control circuits can be used [17], whose design is left for a future study.

IV. Conclusion

This paper has proposed a new A-source impedance network for realizing converters that demand a high voltage gain, while maintaining a small duty ratio and turns ratio of coupled magnetics. An example dc–dc converter has been tested, whose high gain obtained can benefit renewable source interfacing to either a dc or an ac grid. The latter will require an additional dc–ac inverter, implemented as either a single- or double-stage solution. The anticipated network performance features have been tested through simulation and experiment. The results obtained are in close agreement with the theoretically derived. Compared to other existing MCIS networks, the performance demonstrated by the proposed network are presently unmatched, as quantified through detailed mathematical derivation. Considering the significance of control aspects, a small-signal model and control-to-capacitor voltage transfer function is also derived and validated.

References

[1] Y. P. Siwakoti, F. Z. Peng, F. Blaabjerg, P. C. Loh, and G. E. Town, "Impedance source network for electric power conversion—Part I: A topological review," *IEEE Trans. Power Electron.*, vol. 30, no. 2, pp. 699–716, Feb. 2015.

[2] Y. P. Siwakoti, F. Blaabjerg, and P. C. Loh, "New magnetically coupled impedance (Z-) Source networks," *IEEE Trans. Power Electron.*, DOI: 10.1109/TPEL.2015.2459233, Jun. 2015.

[3] A. Chub, D. Vinnikov, F. Blaabjerg, and F. Z. Peng, "A review of galvanically isolated impedance-source DC–DC converters," *IEEE Trans. Power Electron.*, vol. 31, no. 4, pp. 2808–2828, Apr. 2016.

[4] P. C. Loh, D. Li, and F. Blaabjerg, "Γ-Z-source inverters," *IEEE Trans. Power Electron.*, vol. 28, no. 11, pp. 4880–4884, Nov. 2013.

[5] R. Strzelecki, M. Adamowicz, N. Strzelecka, and W. Bury, "New type T-source inverter," in *Proc. Compatibilty Power Electron.*, May 2009, pp. 191–195.

[6] W. Qian, F. Z. Peng, and H. Cha, "Trans-Z-source inverters," *IEEE Trans. Power Electron.*, vol. 26, no. 12, pp. 3453–3463, Dec. 2011.

[7] M. K. Nguyen, Y. C. Lim, and Y. G. Kim, "TZ-source inverters," *IEEE Trans. Ind. Electron.*, vol. 60, no. 12, pp. 5686–5695, Dec. 2013.

[8] M. Adamowicz, R. Strzelecki, F. Z. Peng, J. Guzinski, and A. H. Rub, "New type LCCT-Z-source inverters," in *Proc. 14th Eur. Power Conf. Power Electron. Appl.*, Sep. 2011 pp. 1–10.

[9] M. Adamowicz, J. Guzinski, and P. Stec, "Five-phase EV drive with switched-autotransformer (LCCAt) inverter," in *Proc. IEEE Veh. Power Orpulsion Conf.*, Oct. 2014, pp. 1–6.

[10] Y. P. Siwakoti, P. C. Loh, F. Blaabjerg, S. J. Andreasen, and G. E. Town, "Y-Source impedance network based boost DC/DC converter for distributed generation," *IEEE Trans. Ind. Electron.*, vol. 62, no. 2, pp. 1059–1069, Feb. 2015.

[11] P. C. Loh, D. M. Vilathgamuwa, C. J. Gajanayake, Y. R. Lim, and C. W. Teo, "Transient modeling and analysis of pulse-width modulated Zsource inverter," *IEEE Trans. Power Electron.*, vol. 22, no. 2, pp. 498–507, Mar. 2007.

[12] M. Forouzesh, Y. P. Siwakoti, F. Blaabjerg, and S. Hasanpour, "Small signal modeling and comprehensive analysis of magnetically coupled impedance source converters," *IEEE Trans. Power Electron.*, DOI: 10.1109/TPEL.2016.2553849, Apr. 2016.

[13] R. D. Middlebrook and S. Cuk, "A general unified approach to modelling switching-converter power stages," in *Proc. IEEE Power Electron. Spec. Conf.*, Cleveland, OH, USA, Jun. 1976, pp. 18–34.

[14] D. Czarkowski and M. K. Kazimierczuk, "Energy conservation approach to modeling PWM DC-DC converters," *IEEE. Trans. Aerosp. Electron. Syst.*, vol. 29, no. 3, pp. 1059–1063, Jul. 1993.

[15] V. P. Galigekere and M. K. Kazimierczuk, "Small-signal modeling of open-loop PWM Z-source converter by circuit-averaging technique," *IEEE Trans. Power Electron.*, vol. 28, no. 3, pp. 1286–1296, Mar. 2013.

[16] A. Ayachit, A. Reatti, and M. K. Kazimierczuk, "Small-signal modeling of the PWM boost DC-DC converter at boundary-conduction mode by circuit averaging technique," in *Proc. IEEE Int. Symp. Circuits Syst.*, Lisbon, Portugal, May 2015, pp. 229–232.

[17] B. Bryant and M. K. Kazimierczuk, "Voltage loop of boost PWM DC-DC converters with peak current-mode control," *IEEE Trans. Circ. Syst. – I: Regular Papers*, vol. 53, no. 1, pp. 99–106, Jan. 2006.